6
Absolute Neutrino Masses

6.1
Preliminaries

As we have seen, neutrino oscillation data provide information on the three neutrino mixing angles as well as the two independent neutrino squared mass splittings. However, they are insensitive to the absolute scale of neutrino masses. There are three main approaches towards probing the latter:

1) studies of the shape of the endpoint spectrum in tritium β decays;
2) searches for neutrinoless double-beta decay;
3) measurements of cosmological observables, such as those associated with the cosmic microwave background.

In this chapter, we focus on beta and double-beta decays. The cosmological sensitivity to absolute neutrino mass depends upon which set of observables is included, and is improving fast, with an important impact of data from the PLANCK mission [90]. For a detailed analysis of this, there are excellent textbooks on neutrino cosmology; for a recent one, see, for example, Ref. [4].

6.2
Beta-Decay and Direct Searches for Neutrino Mass

Beta-decay studies provide the classical way to probe '$\overline{\nu}_e$ mass' directly. Historically, this process has also played a major role, since it gave the motivation for Pauli to introduce the neutrino. Many fundamental properties of the weak interactions were discovered by studying beta decays.

Beta decay is a nuclear transition in which the atomic number Z of the nucleus changes by one unit while the atomic mass A remains the same. There are three possible decay varieties: β^- and β^+ decays and electron capture, given by

$$\begin{aligned}
&(A,Z) \to (A,Z+1) + e^- + \overline{\nu}_e,\\
&(A,Z) \to (A,Z-1) + e^+ + \nu_e,\\
&e^- + (A,Z) \to (A,Z-1) + \nu_e.
\end{aligned} \tag{6.1}$$

Neutrinos in High Energy and Astroparticle Physics, First Edition. José W. F. Valle and Jorge C. Romão.

The basic underlying process engendering these nuclear conversions is

$$n \to p + e^- + \overline{\nu}_e, \tag{6.2}$$

which corresponds to $d \to u + e^- + \overline{\nu}_e$ at the quark level. There are excellent textbooks describing the physics of beta decays (see, e.g. Ref. [292]), so here we focus on tritium beta decay. Currently, great effort is under way to get information on the effective 'mass of the electron anti-neutrino' using tritium beta decay as in the KATRIN (KArlsruhe TRItium Neutrino) experiment [293–295]. The aim is to scale up the size and improve the sensitivity of previous experiments by an order of magnitude. This requires an increase in the intensity of the tritium beta-decay source and constitutes a major step forward in the use of the tritium endpoint method.

6.2.1
Relativistic Beta-Decay Kinematics

We now briefly discuss the kinematics relevant for the determination of neutrino masses from the shape of the endpoint spectrum within a fully relativistic approach [296]. In what follows, we label the relativistic momenta and energies involved in tritium beta decay according to

$$^3H(\mathbf{0}, M) \to {}^3He^+(\boldsymbol{p'}, E') + e^-(\boldsymbol{p_e}, E_e) + \overline{\nu}_e(\boldsymbol{p_\nu}, E_\nu). \tag{6.3}$$

The masses of $^3He^+$, e^- and $\overline{\nu}_e$ are denoted by M', m_e and m_ν, respectively. In order to carry out the full phase space integration using relativistic kinematics, we start from the standard formula for the decay width at rest, namely

$$\Gamma = \frac{1}{2^9\pi^5 M}\int \frac{d^3p_e d^3p_\nu d^3p'}{E_e E_\nu E'} |\mathcal{M}|^2 \delta^4(p_{\text{initial}} - p' - p_e - p_\nu), \tag{6.4}$$

where $|\mathcal{M}|^2$ denotes the spin-summed Lorentz-invariant 'squared' amplitude. In order to explore the constraint of Lorentz Invariance, one might *a priori* consider expanding $|\mathcal{M}|^2$ in terms of invariants constructed out the four momenta. For example, up to two powers of momenta, one has

$$|\mathcal{M}|^2 = A - Bp_e \cdot p_\nu - Cp' \cdot p_{\text{initial}} + \cdots, \tag{6.5}$$

where A, B and C are constants. Now it is easy to perform some initial integrations. As usual, $\int d^3p'$ is first performed with the momentum delta function. Then, the angle between $\boldsymbol{p}_e$ and $\boldsymbol{p}_\nu$ is eliminated using the energy delta function. Three more angular integrals are trivial. As a result, one may replace in the ^3H rest frame

$$|\mathcal{M}|^2 \to A + B(E_e E_\nu - \boldsymbol{p}_e \cdot \boldsymbol{p}_\nu) + CM(M - E_e - E_\nu), \tag{6.6}$$

where

$$\boldsymbol{p}_e \cdot \boldsymbol{p}_\nu \equiv M^2 - M'^2 + m_e^2 + m_\nu^2 - 2ME_e + 2E_\nu(E_e - M). \tag{6.7}$$

Equation (6.6) can now be inserted in the resulting usual formula [21]

$$\Gamma = \frac{1}{2^6\pi^3 M}\int dE_\nu dE_e |\mathcal{M}|^2. \tag{6.8}$$

Next we find $d\Gamma/dE_e$ by integrating over dE_ν for each E_e. The limits of integration $E_\nu^{\min}(E_e)$ and $E_\nu^{\max}(E_e)$ can be obtained from [21]. The most tedious part of the calculation consists in finding the factorizations

$$E_\nu^{\max} - E_\nu^{\min} = \frac{2Mp_e}{(m_{12})^2}(E_e^{\max} - E_e)^{1/2}\left[E_e^{\max} - E_e + \frac{2m_\nu M'}{M}\right]^{1/2}, \tag{6.9}$$

$$E_\nu^{\max} + E_\nu^{\min} = \frac{2M}{(m_{12})^2}(M - E_e)\left[E_e^{\max} - E_e + \frac{m_\nu}{M}(M' + m_\nu)\right], \tag{6.10}$$

where

$$(m_{12})^2 = M^2 - 2ME_e + m_e^2. \tag{6.11}$$

The use of the factorization makes the behaviour at the endpoint $E_e = E_e^{\max}$ very transparent. One finds the exact relativistic result

$$\begin{aligned}\frac{d\Gamma}{dE_e} =& \frac{1}{(2\pi)^3}\frac{p_e}{4(m_{12})^2}\sqrt{y\left(y + \frac{2m_\nu M'}{M}\right)}\left[A + CM(M - E_e)\right.\\ &+ BM\frac{ME_e - m_e^2}{(m_{12})^2}\left(y + \frac{m_\nu}{M}(M' + m_\nu)\right)\\ &\left.-C\frac{M^2}{(m_{12})^2}(M - E_e)\left(y + \frac{m_\nu}{M}(M' + m_\nu)\right)\right],\end{aligned} \tag{6.12}$$

where $y = E_e^{\max} - E_e$. As it stands, this formula is based only on the kinematic assumption in Eq. (6.5). One sees that it clearly vanishes at the endpoint $y = 0$ as $\sqrt{y}$. Note that all other terms are finite at $y = 0$. The overall factor $\sqrt{y(y + 2m_\nu M'/M)}$ gives the behaviour of $\frac{d\Gamma}{dE_e}$ extremely close to $y = 0$ for any choice of A, B and C, though it departs from $\frac{d\Gamma}{dE_e}$ away from the endpoint. Dynamics enters in the picture through the coefficients A, B and C.

Using the conventional procedure, one obtains a Lorentz non-invariant term [297],

$$|\mathcal{M}|^2 = BE_eE_\nu, \tag{6.13}$$

which is in excellent agreement with our fully relativistic approach.[1)] This corresponds to having

$$A = C = 0, \quad B \neq 0. \tag{6.14}$$

A more detailed treatment of the underlying interaction dynamics might give rise to small non-zero A and C as well as other unwritten coefficients in Eq. (6.5) above. The relativistic form for the spectrum shape near the endpoint becomes

$$\frac{d\Gamma}{dE_e} = \frac{p_eMB}{(2\pi)^3 4(m_{12})^4}(ME_e - m_e^2)\sqrt{y\left(y + \frac{2m_\nu M'}{M}\right)}\left[y + \frac{m_\nu}{M}(M' + m_\nu)\right]. \tag{6.15}$$

1) This follows from taking the spin sum for a four-fermion interaction, for a constant nuclear matrix element.

Note that, if we had employed the non-relativistic form given in Eq. (6.13), the net result would be a replacement of an overall factor in Eq. (6.15) according to

$$(ME_e - m_e^2) \to (ME_e - E_e^2). \tag{6.16}$$

The difference of these two factors yields the contribution of the $\boldsymbol{p}_e \cdot \boldsymbol{p}_\nu$ term, which is tiny near the endpoint region since it is proportional to p_e^2 and is suppressed like $p_e^2/(ME_e)$ compared to unity. If we further approximate $M'/M \to 1$ and $\frac{M'+m_\nu}{M} \to 1$, the endpoint shape is well described by

$$\frac{d\Gamma}{dE_e} \quad \propto \quad (y + m_\nu)\sqrt{y(y + 2m_\nu)}. \tag{6.17}$$

Now, comparing with the formula used in the experimental analysis [298], namely

$$\frac{d\Gamma}{dE_e} \quad \propto \quad (E_0 - V_i - E)\sqrt{(E_0 - V_i - E)^2 - m_\nu^2}, \tag{6.18}$$

one sees that it agrees with the approximation in Eq. (6.17) provided one identifies

$$(E_0 - V_i - E) = y + m_\nu. \tag{6.19}$$

Note that E is the non-relativistic energy given by $E = E_e - m_e$. Furthermore, $E_0 - V_i$ is identified with our $(M - M' - m_e - \delta E_e^{\max})$, while $\delta E_e^{\max}$ is defined by

$$E_e^{\max} = M - M' - m_\nu - \delta E_e^{\max}, \tag{6.20}$$

and is independent of m_ν to a good approximation [299]. Thus we see that the 'exact' relativistic endpoint obtained here is well approximated by the form used in the experimental analysis. Results are often expressed in terms of x, defined as

$$x = -y - m_\nu = E_e - E_e^{\max} - m_\nu. \tag{6.21}$$

In Figure 6.1, $d\Gamma/dE_e$ as computed from the 'exact' formula, Eq. (6.15), is compared with its approximate analogue as a function of x. As can be seen, the differences between the approximate and exact formulas are very small.

Realistic Monte Carlo simulations for the tritium experiment KATRIN can be performed using the exact relativistic kinematic expression in Eq. (6.15) for neutrino masses of $m_\nu = 0$ eV and $m_\nu = 1$ eV and the standard formula (Eq. (6.18)) with excellent agreement [296].

6.2.2
Beta Decay in the Three-Neutrino Case

We now consider the case of three generations of neutrinos with different masses m_1, m_2 and m_3, and the resulting impact of neutrino oscillation data upon the expectations for the beta-decay endpoint counting rates for the different types of

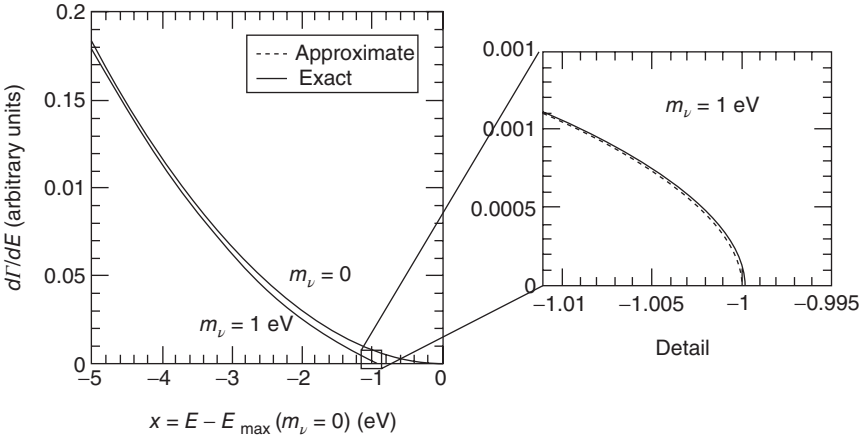

Figure 6.1 Effect of neutrino mass in tritium endpoint: approximate versus exact relativistic result. Taken from [296].

neutrino mass spectra. Then, there will be a different endpoint energy, $E_i^{\max}$, corresponding to each one. The effective endpoint factor in the good approximation of Eq. (6.17) is the weighted sum

$$F_{eff}(E_e) = \sum_{i=1}^{3} |K_{1i}|^2 (y_i + m_i)[y_i(y_i + 2m_i)]^{1/2}\theta(y_i), \tag{6.22}$$

where $y_i(E_e) = E_i^{\max} - E_e$ and the K_{1i} are the elements of the 3×3 lepton mixing matrix. We note that the further good approximation, namely the quantity $\delta E_e^{\max}$ is independent of the neutrino mass, gives the useful relation

$$y_i - y_j = m_j - m_i. \tag{6.23}$$

Now, let the unindexed quantity y stand for the y_i with the smallest of the neutrino masses. Using Eq. (6.23) allows us to write the explicit formula for the case (denoted 'normal hierarchy') where m_1 is the lightest of the three neutrino masses as

$$\begin{aligned} F_{NH}(y) = {} & |K_{11}|^2 (y + m_1)[y(y + 2m_1)]^{1/2} \\ & + |K_{12}|^2 (y + m_1)[(y + m_1 - m_2)(y + m_1 + m_2)]^{1/2}\theta(y + m_1 - m_2) \\ & + |K_{13}|^2 (y + m_1)[(y + m_1 - m_3)(y + m_1 + m_3)]^{1/2}\theta(y + m_1 - m_3). \end{aligned} \tag{6.24}$$

In the other case of interest (denoted 'inverse hierarchy'), we have

$$\begin{aligned} F_{IH}(y) = {} & |K_{13}|^2 (y + m_3)[y(y + 2m_3)]^{1/2} \\ & + |K_{11}|^2 (y + m_3)[(y + m_3 - m_1)(y + m_3 + m_1)]^{1/2}\theta(y + m_3 - m_1) \\ & + |K_{12}|^2 (y + m_3)[(y + m_3 - m_2)(y + m_3 + m_2)]^{1/2}\theta(y + m_3 - m_2), \end{aligned} \tag{6.25}$$

where m_3 is the lightest of the three neutrino masses. From these equations, we may easily find the counting rate in the energy range from the appropriate endpoint up to $y_{\max}$ as proportional to the integral

$$n_{NH}(y_{\max}) = \int_0^{y_{\max}} dy F_{NH}(y), \tag{6.26}$$

or, for the 'inverse hierarchy' case, as proportional to

$$n_{IH}(y_{\max}) = \int_0^{y_{\max}} dy F_{IH}(y). \tag{6.27}$$

Note that, as stressed in Ref. [299], information on neutrino masses and mixings obtained from neutrino oscillation experiments is actually sufficient, in principle, to predict $n(y_{\max})$ as a function of a single parameter (up to a two-fold ambiguity). Thus, in principle, suitably comparing the predicted values of $n(y_{\max})$ with results from a future endpoint experiment may end up determining three neutrino masses.

To see how this might work out, we make an initial estimate using the latest best fit values [83] of neutrino squared mass differences

$$\begin{aligned} \text{solar} &\equiv m_2^2 - m_1^2 = 7.62 \times 10^{-5}\text{eV}^2, \\ \text{atmospheric} &\equiv |m_3^2 - m_1^2| = 2.55 \times 10^{-3}\text{eV}^2 \qquad \text{NH}, \\ &\quad\; |m_3^2 - m_1^2| = 2.43 \times 10^{-3}\text{eV}^2 \qquad \text{IH}, \end{aligned} \tag{6.28}$$

and the lepton mixing matrix coefficients

$$|K_{11}|^2 = 0.66, \qquad |K_{12}|^2 = 0.31, \qquad |K_{13}|^2 = 0.025. \tag{6.29}$$

Now, given the differences in Eq. (6.28), for each choice of m_3 (considered as our free parameter) one can find the masses m_1 and m_2, subject to the ambiguity as to whether m_3 is the largest (NH) or the smallest (IH) of the three neutrino masses. Of course, one hopes that future long-baseline neutrino oscillation experiments [300–303] will eventually determine whether Nature prefers the NH or the IH scenario.

Figure 6.2 shows typical solutions for the mass set (m_1, m_2) in terms of the free parameter m_3. Very large values of m_3 would fall within the sensitivity of cosmological observations [4]. In Figure 6.2b, we display the predicted values of $n(y_{\max})$ for each possible mass scenario and the choices of $(1, 10, 20)$ eV for $y_{\max}$. These quantities are proportional to the electron counting rate in the energy range from the endpoint (for each mass scenario) to $y_{\max}$ (eV) below the endpoint. The different values of $y_{\max}$ reflect, of course, different experimental sensitivities. The main point is that, for sufficiently large m_3 values, the counting rate is seen to distinguish the different possible neutrino mass sets from each other.

In summary, we showed that the absolute neutrino mass scale has an effect upon the beta-decay endpoint spectrum. We did this using a very simple and useful factorized and exact relativistic form, which can be very well approximated by the endpoint form used by the KATRIN collaboration. We have also discussed the

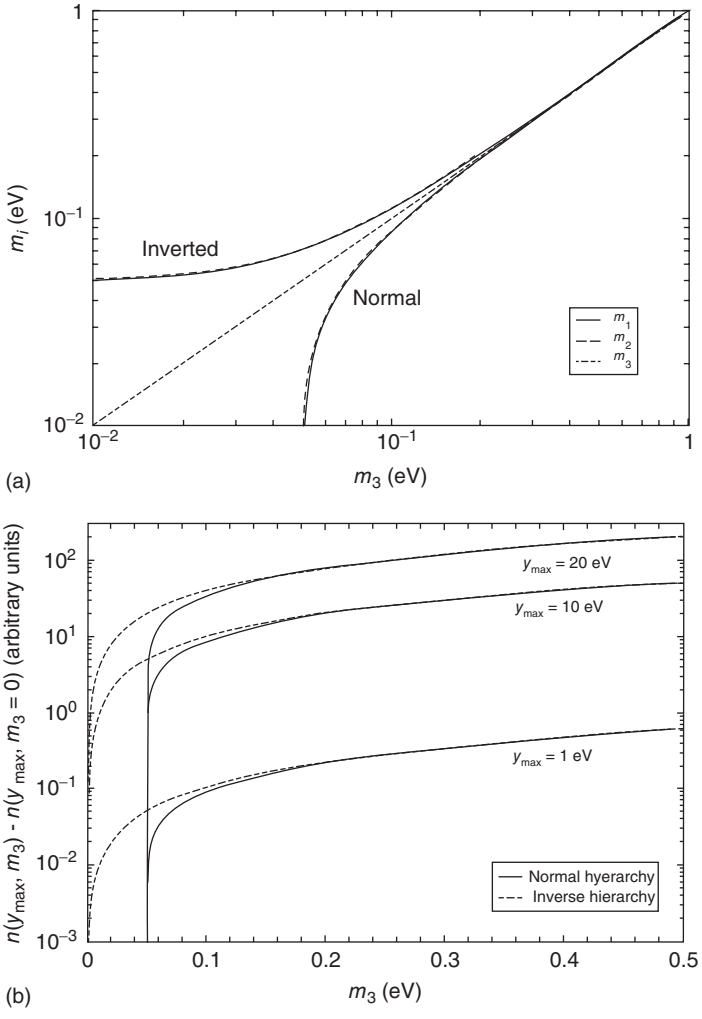

Figure 6.2 (a) Typical solutions for (m_1, m_2) as a function of m_3 for the NH case (solid curves) and the IH case (dashed curves); the middle dot-dashed is given for orientation. (b) The predictions for the quantities, $n(y_{\max})$, proportional to the event counting rate which includes emitted electrons within 1, 10 and 20 eV from the appropriate endpoint, respectively. Taken from [296].

three-neutrino case and shown how to incorporate information from neutrino oscillation experiments in the analysis of beta-decay endpoint experiments. One hopes that the impact of the observed neutrino oscillation parameters upon the predictions for the beta-decay endpoint counting rates may play a useful role in future experiments.

6.3
Neutrinoless Double-Beta Decay

In this section we consider double-beta decay. This process is induced as a second-order weak interaction. In two-neutrino double-beta decay or $2\nu\beta\beta$, one has

$$(A, Z) \to (A, Z+2) + 2e^- + 2\overline{\nu}. \tag{6.30}$$

That is, two neutrons in a nucleus are converted to protons, emitting two electrons plus two electron anti-neutrinos, see Figure 6.3a. In other words, $2\nu\beta\beta$ is a doubly weak process in which two neutrons in the nucleus undergo beta decay. The final nucleus should have a larger binding energy than the original one. For some nuclei, such as ^{76}Ge, it happens that the nucleus with atomic number one higher has a smaller binding energy, preventing a single beta decay from taking place. However, the nucleus with atomic number two higher, ^{76}Se, has a larger binding energy, so the double-beta decay process is allowed. This process is ordinary in the sense that it conserves lepton number. Yet, it is the rarest known kind of radioactive decay, and only after several decades of experimental efforts has it been observed in ^{82}Se [304] and by now in more than ten other nuclei including ^{76}Ge [102, 103]. Recently, the EXO-200 and KamLAND-ZEN collaborations have detected the $\beta\beta_{2\nu}$ of ^{136}Xe [305, 306].

Because of its basic conceptual importance as the only potentially feasible way of probing the nature – Dirac or Majorana – of neutrinos [87, 88], let us concentrate on neutrinoless double-beta decay or $0\nu\beta\beta$. This is the second-order nuclear beta-decay process [104]

$$(A, Z) \to (A, Z+2) + 2e^-, \tag{6.31}$$

in which no neutrino is emitted in the final state: rather, there is a virtual neutrino (or a combination) which is exchanged *between* the decaying neutrons, as illustrated in Figure 6.3b.

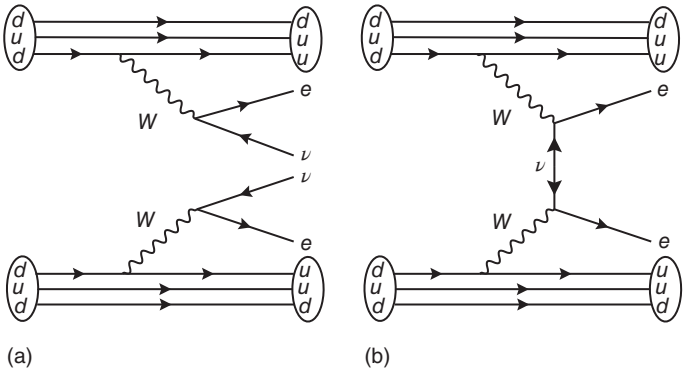

Figure 6.3 Feynman diagram for the lepton-number-conserving Double-beta decay (a) and diagram generating $0\nu\beta\beta$ decay from light neutrino exchange (b).

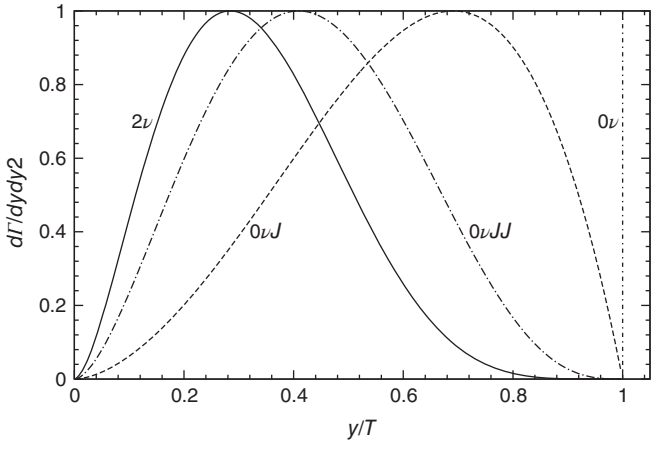

Figure 6.4 Shape of differential electron spectrum characterizing ordinary $2\nu\beta\beta$ (solid) and various types of lepton-number-violating double beta decay: $0\nu\beta\beta$ (dot-dashed peak), $0\nu J$ (dashed curve) and $0\nu JJ$ (dot-dashed curve).

The corresponding quark-level effective dimension-9 operator is given as

$$\mathcal{O}_{0\nu\beta\beta} \propto \bar{u}\,\bar{u}\,dd\,\bar{e}\,\bar{e}, \tag{6.32}$$

which may contain both long- and short-range contributions (see Section 6.7).

What is usually measured in experiment is the differential electron spectrum which is the sum of the kinetic energies of the two electrons expressed in units of the electron mass. The resulting shapes are shown in Figure 6.4. The continuous spectrum given by the solid curve corresponds to the ordinary $2\nu\beta\beta$ decay. The lepton-number-violating $0\nu\beta\beta$ decay labelled 0ν corresponds to the dot-dashed peak at the endpoint. On the other hand, the 'intermediate' continuous shapes labelled $0\nu J$ and $0\nu JJ$ are associated with new varieties of lepton-number-violating neutrinoless double-beta decay involving majoron emission processes, illustrated in Figure 6.5.

The left panel corresponds to single majoron emission and exists when the majoron carries two units of lepton number, like the seesaw majoron model to be discussed in Chapter 7. As we will see in Section 7.3, such a single emission process may be sizeable only for seesaw schemes where lepton number is spontaneously violated at a very low scale. On the other hand, models such as supersymmetry with spontaneously broken R-parity, the majoron carries only one unit of lepton number, as will be discussed in Chapter 10. As a result, such schemes lead to this variety of neutrinoless double- beta decay, where the effective dimension-5 JJ$\nu\nu$ coupling arises from electroweak gaugino exchanges. This leads to expected decay rates which are typically too small to be of interest.

Before closing this discussion, let us mention that the angular distribution of the electrons emitted in the decay is also relevant, as it is sensitive to the nature of the mechanism inducing neutrinoless double-beta decay [102, 103].

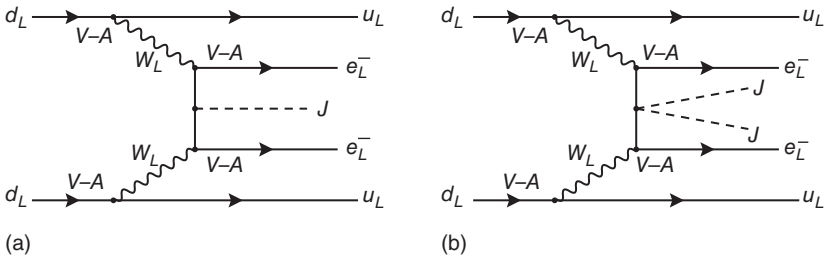

Figure 6.5 Feynman diagrams for majoron-emitting neutrinoless double- beta decay mechanisms. (a) Majoron with $\Delta L = 2$ and (b) majoron with $\Delta L = 1$.

The search for lepton-number-violating processes such as $0\nu\beta\beta$ opens the way to probe the basic nature of neutrinos and also the CP violation induced by the so-called Majorana phases [46]. As already mentioned in Problems 4.2 and 4.3 of Chapter 4, the latter do not show up in conventional neutrino oscillation experiments [172, 173] but can affect lepton-number-violating processes [171] such as neutrinoless double-beta decays [185] and electromagnetic properties of neutrinos [169, 170]. Nevertheless, $0\nu\beta\beta$ searches seem closer to being realistic at the moment than searches for Majorana CP violation.

6.4
Light-Neutrino Exchange $0\nu\beta\beta$ Mechanism

As illustrated in Figure 6.3b, the most direct way of inducing $0\nu\beta\beta$ is the so-called mass mechanism involving the exchange of massive Majorana neutrinos. Given that neutrino masses have been experimentally confirmed in oscillation experiments, we expect that there is a contribution to $0\nu\beta\beta$ involving the exchange of light Majorana neutrinos, namely the 'mass mechanism'. The associated amplitude is proportional to

$$m_{\beta\beta} = \sum_i K_{ei}^2 m_i, \tag{6.33}$$

where the parameters K_{ei} form the first row in the lepton mixing matrix. An important feature of this amplitude is that it involves the lepton-number-violating propagator in Eq. (3.20) and, as a result, none of the K_{ei} factors that appears in Eq. (6.33) has complex conjugation. From it follows that Majorana phases can have an important effect, leading to the possible destructive interference among amplitudes arising from different neutrino types. In fact, such destructive interferences may also take place without the need for CP violation [185]. This is what happens, for example, in the case of a pure Dirac neutrino; the exact cancellation coming in this case from the phase present in Eq. (3.14) reflects the conservation of lepton number which, as expected, forbids the process. Partial cancellations of the $0\nu\beta\beta$ decay amplitude induced by the exchange of two neutrinos as a result of a quasi-conserved lepton number symmetries are possible. Depending on their

$SU(3)_c \otimes SU(2)_L \otimes U(1)_Y$ transformation properties, different limiting cases can be considered. For example, a quasi-Dirac neutrino is one made up of one active and one sterile component, almost degenerate in mass due to the nearly exact conservation of standard lepton number [307]. In other words, a system of two neutrinos in which one is a gauge singlet and the other an isodoublet with almost degenerate mass eigenstates.[2] This leads to the possibility of active-to-sterile neutrino oscillations. Depending on the size of the mass splitting, such conversions in the early Universe may, for example, affect primordial Big Bang Nucleosynthesis predictions [4].

On the other hand, Wolfenstein introduced the concept of a pseudo-Dirac neutrino made up of two $SU(2)_L$ doublet (active) neutrinos, nearly degenerate as a result of the approximate conservation of some non-standard combination of lepton numbers [309]. He noted that a cancellation of the $0\nu\beta\beta$ decay amplitude also exists even if the two neutrinos are not close in mass, provided the *ee* element of the neutrino mass matrix in the weak basis vanishes [309].

An adequate parameterization of the Majorana phases in Eq. (6.33) will be helpful in interpreting the effective mass parameter characterizing the amplitude for neutrinoless double-beta decay. One finds

$$m_{\beta\beta} = \begin{cases} \left| c_{12}^2 c_{13}^2\, m_1 + s_{12}^2 c_{13}^2\, m_2\, e^{\frac{1}{2} i\alpha_{21}} + s_{13}^2\, m_3\, e^{\frac{1}{2} i(\alpha_{31} - 2\delta)} \right| & \text{(PDG)}, \\ \left| c_{12}^2 c_{13}^2\, m_1 + s_{12}^2 c_{13}^2\, m_2\, e^{2i\phi_{12}} + s_{13}^2\, m_3\, e^{2i\phi_{13}} \right| & \text{(symm)}, \end{cases} \tag{6.34}$$

where α_{21}, α_{31} and δ are the three CP phases within the PDG (Particle Data Group) convention [21].

Note that this amplitude is sensitive to the absolute scale of neutrino mass, and depends upon two of the mixing angles in the lepton mixing matrix as well as on the two Majorana CP phases that characterize the minimal three-neutrino mixing matrix [46], none of which can be probed in oscillations. Note also that, as expected, only the two basic Majorana phases appear in $m_{\beta\beta}$ if one uses the original symmetrical parameterization [46]. In contrast, this is not at all clear within the PDG presentation. Hence, the symmetrical parameterization provides a more transparent description in which only the two basic Majorana phases appear in $m_{\beta\beta}$, as it should.[3]

This amplitude may be plotted graphically versus the lightest neutrino mass, as illustrated in Figure 6.6, which shows the estimated average mass parameter $m_{\beta\beta}$ characterizing the neutrino exchange contribution to $0\nu\beta\beta$ versus the lightest neutrino mass. The calculation takes into account the current neutrino oscillation parameters in [83]. The dark and grey bands correspond to the generic cases of normal and inverted mass hierarchy, respectively. In contrast to normal hierarchy, where full destructive interference amongst the three light neutrinos is possible, for the inverted case the $0\nu\beta\beta$ amplitude never vanishes. Note that the neutrino

2) The mass splittings between the two neutrinos may be radiatively calculable [308].
3) Recall that what corresponds to the Dirac phase which appears in conventional neutrino oscillations is the rephasing-invariant combination $\phi_{13} - \phi_{12} - \phi_{23}$, see Problem 4.2.

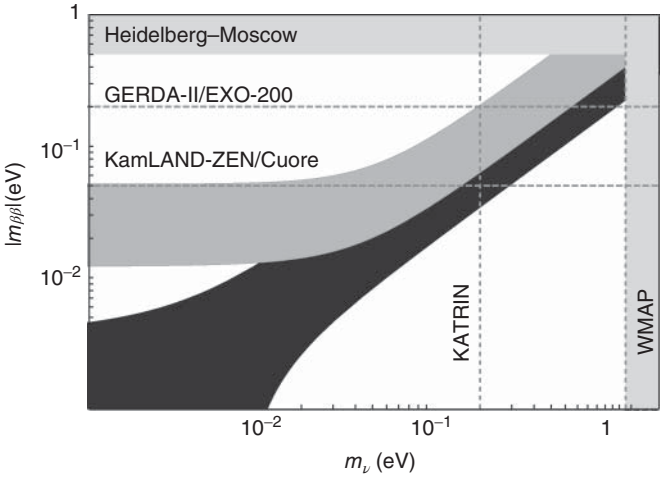

Figure 6.6 Neutrinoless double-beta decay effective amplitude parameter versus the lightest neutrino mass in a generic model. A summary of experimental sensitivities is shown for comparison.

Table 6.1 Current published $0\nu\beta\beta$ limits for various isotopes, with the QRPA nuclear matrix elements [315].[a)]

	^{A}Z	Location	$T_{1/2}^{0\nu\beta\beta}$ (yr)	$m_{\beta\beta}$ (eV)	Year	References
Hd-Mo	^{76}Ge	LNGS	1.9×10^{25}	0.35	2001	[310]
IGEX	^{76}Ge	Canfranc	1.6×10^{25}	0.38	2002	[311]
Cuoricino	^{130}Te	LNGS	2.94×10^{24}	0.40	2008	[312]
NEMO-III	^{100}Mo	LSM	1.1×10^{24}	1.1	2010	[313]
EXO-200	^{136}Xe	WIPP	1.6×10^{25}	0.34	2012	[314]
KamLAND-ZEN	^{136}Xe	Kamioka	1.9×10^{25}	0.32	2012	[306]

a) Courtesy of M. Hirsch.

oscillation parameters are taken at 3σ, while Majorana phases are allowed to vary between their extreme values. The two rising bands overlap in the 'diagonal' region corresponding to the case of quasi-degenerate neutrinos predicted by some models [113]. This gives the largest possible $0\nu\beta\beta$ amplitude.

The current experimental sensitivities to the $0\nu\beta\beta$ half-lives of various nuclear isotopes are summarized in Table 6.1. In order to extract the physics information encoded in the parameter $m_{\beta\beta}$, one requires a precise knowledge of the nuclear matrix elements [315, 316], still typically uncertain by about a factor of two.

We indicate in the horizontal band in Figure 6.6 the limit from the Heidelberg–Moscow experiment [310], and in the vertical band we show the region disfavoured by cosmological arguments [4]. The horizontal and vertical lines indicate future expected sensitivities on $m_{\beta\beta}$ and the lightest neutrino mass, respectively.

Table 6.2 Expected $0\nu\beta\beta$ sensitivities in the near future (roughly: this decade). KamLAND-ZEN is known, from their first measurement, to have currently a much higher background level than used in the proposal [306]. Also, GERDA-I has not yet published results because of background issues. This should be compared with Table 6.1.[a)]

	^{A}Z	Location	$T^{0\nu\beta\beta}_{1/2}$ (yr)	$m_{\beta\beta}$ (eV)
GERDA-II	^{76}Ge	LNGS	1.5×10^{26}	0.12
Cuore	^{130}Te	LNGS	2×10^{26}	0.05
EXO-200	^{136}Xe	WIPP	6.4×10^{25}	0.18
KamLAND-ZEN	^{136}Xe	Kamioka	6.0×10^{26}	0.06
SNO+	^{150}Nd	Sudbury	1.5×10^{24}	0.15
NEXT	^{136}Xe	Canfranc	5.9×10^{25}	0.18

a) Courtesy of M. Hirsch.

6.5
Experimental Prospects in the Search for $0\nu\beta\beta$

Future experiments will extend the sensitivity of current $0\nu\beta\beta$ searches beyond the present levels. We now turn to the expectations from the upcoming experiments, which are summarized in Table 6.2.[4)] The compilation is taken from the proposals; therefore, the background indices are not experimentally known but only from Monte Carlo simulations. Note that the numbers in the last row in Table 6.2 are based on the somewhat optimistic assumption that a background index of 8×10^{-4} in units of (keV kg year) can be reached. The improved sensitivities expected for some experiments of the next generation are compiled in Table 6.3.

6.6
Neutrinoless Double-Beta Decay in Flavour Models

Understanding the pattern of neutrino mixing inferred from neutrino oscillation experiments constitutes one of the current challenges in particle physics and forms part of the so-called flavour problem, which is one of the deepest in the field. Although the observed angles might result accidentally, it seems reasonable to expect that their pattern should be explained from first principles. Here we comment on how the underlying flavour structure which accounts for the observed pattern of neutrino oscillations may have some impact on the $0\nu\beta\beta$ amplitude. As a simple example, we mention the possibility of having (nearly) degenerate neutrinos as a result of the flavour symmetry of the model [113], implying a stringent lower bound on the absolute neutrino mass $m_\nu \gtrsim 0.4$ eV comparable to current sensitivities.

4) The small differences between some entries in the two tables are due to nuclear matrix elements.

Table 6.3 Sensitivities of future $0\nu\beta\beta$-decay experiments to the effective mass parameter calculated with the RQRPA nuclear matrix elements $M^{0\nu}(A, Z)$ of Ref. [316] taking the axial coupling constant $g_A = 1.25$. $T_{1/2}^{0\nu-\mathrm{exp}}$ is the maximum half-life that can be reached in the experiment, and $|m_{\beta\beta}| \equiv m_{\beta\beta}$ is the corresponding upper limit of the effective Majorana neutrino mass.

Nucleus	Experiment	Source	$T_{1/2}^{0\nu-\mathrm{exp}}$ (yr)	References	$M^{0\nu}(A,Z)$	$\lvert m_{\beta\beta}\rvert$ (eV)
^{76}Ge	GERDA(I)	15 kg of ^{enr}Ge	3×10^{25}	[317]	3.92	0.27
	GERDA(II)	100 kg of ^{enr}Ge	2×10^{26}	[317]	3.92	0.10
	Majorana	0.5 t of ^{enr}Ge	4×10^{27}	[318]	3.92	0.023
^{82}Se	SuperNEMO	100 kg of ^{enr}Se	2×10^{26}	[319]	3.49	0.055
^{100}Mo	MOON	3.4 t of ^{nat}Mo	1×10^{27}	[320]	2.78	0.024
^{116}Cd	CAMEO	1 t of $CdWO_4$ crystals	$\approx 10^{26}$	[320]	2.42	0.085
^{130}Te	CUORE	750 kg of TeO_2	$\approx 10^{27}$	[321]	2.95	0.023
^{136}Xe	XMASS	10 t of liquid Xe	3×10^{26}	[320]	1.97	0.062
					1.67	0.073
	EXO	1 t ^{enr}Xe	2×10^{27}	[322]	1.97	0.024
					1.67	0.028

As seen in Figure 6.6, normal hierarchy schemes generally do not lead to a lower bound for the $0\nu\beta\beta$ amplitude, since the three light neutrinos can interfere destructively and hence suppress the decay rate. However, it has been noted that this cancellation may be prevented even in normal hierarchy schemes, as a result of the interplay of the parameter restrictions implied by the underlying flavour symmetry and the current neutrino oscillation data [83]. Examples of the occurrence of such lower bound have been found in the literature, for example, in Refs [323] and [324].

It has also been noted [325] that many of the models based on non-Abelian discrete flavour symmetries are characterized by a specific (complex) relation between neutrino mass eigenvalues, leading to mass sum rules such as

$$\text{(i)} \qquad \chi\, m_2^\nu + \xi\, m_3^\nu = m_1^\nu, \tag{6.35}$$

$$\text{(ii)} \qquad \frac{\chi}{m_2^\nu} + \frac{\xi}{m_3^\nu} = \frac{1}{m_1^\nu}, \tag{6.36}$$

$$\text{(iii)} \qquad \chi\, \sqrt{m_2^\nu} + \xi\, \sqrt{m_3^\nu} = \sqrt{m_1^\nu}, \tag{6.37}$$

$$\text{(iv)} \qquad \frac{\chi}{\sqrt{m_2^\nu}} + \frac{\xi}{\sqrt{m_3^\nu}} = \frac{1}{\sqrt{m_1^\nu}}. \tag{6.38}$$

Here, $m_i^\nu = m_i^0$ denote neutrino mass eigenvalues, up to a Majorana phase factor, while χ and ξ are free parameters that specify the model, taken to be positive without loss of generality. These can be obtained in flavour models where the neutrino mass matrix depends only on two independent free parameters, so that the resulting mixing angles are fixed, as in the case of tri-bimaximal [249] or bimaximal mixing patterns. For definiteness, here we focus on the case of tri-bimaximal

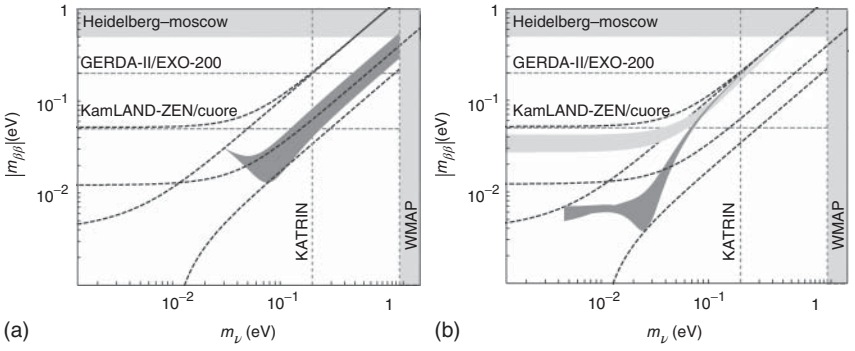

Figure 6.7 (a,b) Neutrinoless double-beta decay effective amplitude parameter versus the lightest neutrino mass in various flavour models. (Adapted from [326, 327].)

neutrino mixing which provides a useful first approximation to the observed pattern of mixing angles. However, when evaluating a lower bound on the effective $0\nu\beta\beta$ decay neutrino mass parameter $m_{\beta\beta}$, we explicitly include the effects of non-vanishing θ_{13} by taking the 3σ oscillation parameter values determined in Ref. [83].

In most cases, these rules lead to lower bounds for the neutrinoless double- beta amplitude parameter [326, 327]. The lower limits on $m_{\beta\beta}$ corresponding to different integer choices of (χ, ξ) between 1 and 3 and for each of the four cases above have been summarized in Table I of Ref. [326] for both normal and inverted hierarchies. They cover a large class of non-Abelian flavour symmetry models discussed in the literature (see Ref. [111] and references therein).

As an example, we display in Figure 6.7 the effective amplitude parameter $m_{\beta\beta}$ characterizing neutrinoless double-beta decay versus the lightest neutrino mass in various flavour models, compared with the generic expectations for each mass ordering.

Within each 'generic' band corresponding to either normal or inverted spectra, the indicated shaded sub-region corresponds to what is allowed within the corresponding neutrino mass sum rule case arising from a particular flavour scheme. Note that, in all three examples, one finds a lower limit for the $0\nu\beta\beta$ amplitude, even within the normal hierarchy case. These lower bounds should, of course, be compared with the expected sensitivities given in Tables 6.2 and 6.3.

6.7 Short-Range Contributions to $0\nu\beta\beta$ Decay and the Weak Interaction Scale

There are two classes of contributions to the $0\nu\beta\beta$ decay rate, short-range [328] and long-range [329] parts. Using simple dimensional analysis, one may characterize the dependence of each type of operator to the new physics scale Λ associated with lepton number violation within a given theory. The light-neutrino exchange mechanism in Figure 6.3b is a long-range contribution and, for this case, one has

very stringent limits on the new physics scale

$$\Lambda \gtrsim \lambda_{\rm LNV}^{\rm eff} \times (10^2 - 10^3)\ {\rm TeV},$$

where $\lambda_{\rm LNV}^{\rm eff}$ characterizes lepton number violation within the model under consideration. This makes it unlikely that one will be able to probe lepton number violation effects at the high energies that are now accessible at the LHC (large hadron collider). In other words, for 'exotic' $0\nu\beta\beta$ mechanisms that fall into this category, the half-life limits from $0\nu\beta\beta$ decay searches provide the most stringent bounds on lepton number violation.

Exotic lepton number violation mechanisms may, however, lead to short-range contributions for $0\nu\beta\beta$ decay. In this case, the $0\nu\beta\beta$ amplitude involves only heavy states with masses at the high energy scale Λ so that, the effective Lagrangian describing $0\nu\beta\beta$ decay is simply proportional to $1/\Lambda^5$. As a result, one may test the new physics leading to $0\nu\beta\beta$ at the LHC energies, since both types of experiments probe new physics at scales so that Λ equal of a few teraelectronvolts. Let us now illustrate this fact with a simple example.

Consider the so-called left–right (LR) symmetric extensions of the standard model [330], based upon the $SU(3)_c \otimes SU(2)_L \otimes SU(2)_R \otimes U(1)$ gauge group. In these models, $0\nu\beta\beta$ decay can be generated in many ways [331], as indicated in Figure 6.8. The amplitude for the process arising from the top-right graph is proportional to

$$\langle m_N \rangle^{-1} \equiv \sum_j V_{ej}^2 / m_{N_j},$$

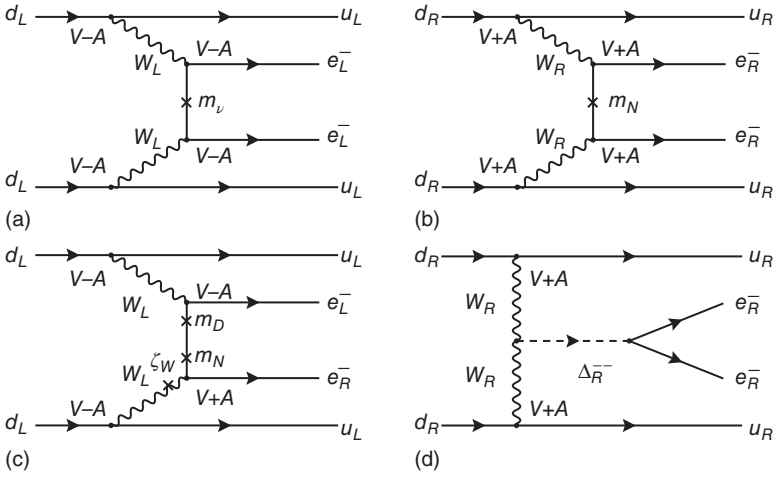

Figure 6.8 Illustrative Feynman diagrams inducing $0\nu\beta\beta$ decay in $SU(3)_c \otimes SU(2)_L \otimes SU(2)_R \otimes U(1)$ theories. (a) The standard light-neutrino mass mechanism and (b) its analogue graph involving (right-handed) neutrino and charged gauge boson W_R exchange. (c) involves a mixed term, while (d) involves the exchange of the isotriplet Higgs boson Δ_R.

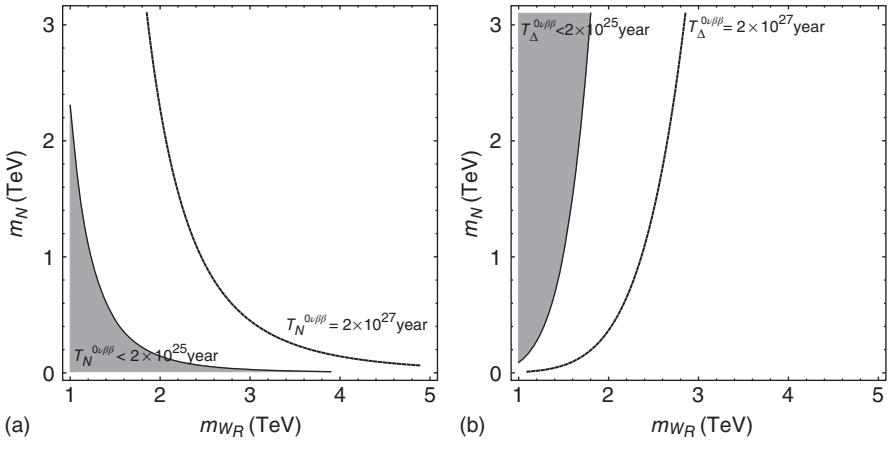

Figure 6.9 Sensitivity of $0\nu\beta\beta$ decays to the relevant mass scales, depending on the dominant mechanism in each case. (a) Right-handed neutrino exchange. (b) Doubly charged Higgs boson exchange. (Updated from [176].)

where V_{ej} are the couplings of the heavy right-handed neutrinos to the electron. Using the nuclear matrix elements of [332], the limit on the half-life [314] corresponds to $\langle m_N \rangle = m_{W_R} \gtrsim 1.3$ TeV (assuming that the gauge coupling of the right-handed and left-handed SU(2)s are equal). This example nicely illustrates the complementarity of $0\nu\beta\beta$ decay searches at underground installations and physics that can be probed at high-energy accelerators such as the LHC.

Indeed, in Figure 6.9 we display the sensitivity of lepton number violation searches to the relevant $SU(3)_c \otimes SU(2)_L \otimes SU(2)_R \otimes U(1)$ mass scales, from Ref. [176]. The shaded areas denote the parameter space excluded by $0\nu\beta\beta$ searches at 2×10^{25} years half-life, assuming dominant heavy neutrino exchange (a) or doubly charged Higgs exchange (b). Clearly, both scales lie in the tera-electronvolt scale, as well as the right-handed gauge boson mass, shown in the abscissa.

The corresponding outer contours show the sensitivity of future $0\nu\beta\beta$ experiments at 2×10^{27} years half-life. In Chapter 13, we will discuss in more detail the associated signals at the LHC as well as the corresponding sensitivities at high energies.

In summary, we have seen that, for the case of short-range contributions, $0\nu\beta\beta$ decay searches are expected to probe physics at the weak interaction scale. We stress that what we gave above is just a classic example of short-range mechanisms that are present in $SU(3)_c \otimes SU(2)_L \otimes SU(2)_R \otimes U(1)$ models. For a systematic decomposition of the neutrinoless double-beta decay operator, focusing on short-range mechanisms with small contributions to neutrino mass but potentially accessible at the LHC, see Ref. [333].

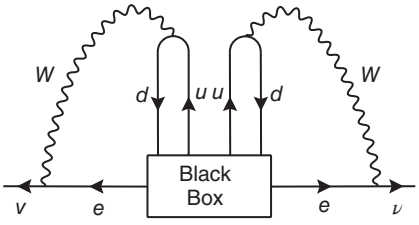

Figure 6.10 Neutrinoless double-beta decay implying that neutrinos are Majorana fermions [87].

6.8
Black Box and the Significance of $0\nu\beta\beta$

As we have seen, within a gauge theory there can be many mechanisms that can engender $0\nu\beta\beta$ other than the neutrino exchange mechanism. Indeed, there can be short-range mechanisms involving the exchange of heavy particles, such as scalar bosons in extended gauge theories [87], particles present in LR or supersymmetric extensions of the standard model [334], and so on. This raises the question of whether indeed the possible observation of $0\nu\beta\beta$ tells us anything about the Majorana nature of neutrinos themselves.

The significance of neutrinoless double-beta decay stems from the fact that, in a gauge theory, irrespective of which is the mechanism that induces $0\nu\beta\beta$, it necessarily implies the existence of a Majorana neutrino mass [87], as illustrated in Figure 6.10.

The validity of this 'theorem' has been recently scrutinized quantitatively in detail in Ref. [88] by considering the most general Lorentz-invariant Lagrangian consisting of point-like operators for neutrinoless double-beta decay. The authors confirm that an observation of $0\nu\beta\beta$ decay ensures the Majorana nature of neutrinos. They calculate the radiative masses generated by the Black Box operators, and find that they are many orders of magnitude smaller than the observed neutrino masses and splittings. If neutrino masses have a significant 'Majorana term', then this will be the dominant part of the Black Box operator and we recover the neutrino exchange mechanism. However, there might be cancellations amongst such mass exchange contributions. This would happen, for example, if neutrinos are quasi-Dirac particles [307]. In such case, other lepton- number-violating new physics contributions could dominate the $0\nu\beta\beta$ decay rate. Translating an observed $0\nu\beta\beta$ rate into neutrino masses would then be completely misleading.

The conclusion is that the Black Box diagram itself generates radiatively only mass terms that are way too small to account for the required neutrino oscillation squared mass splittings. Therefore, other operators must make the leading contributions to neutrino masses.

In summary, in order to derive clean quantitative implications of the Black Box argument, one needs to specify the underlying theoretical model. Although the theorem itself holds in any 'natural' gauge theory, its quantitative impact is strongly model-dependent.

6.9 Summary

Up to this chapter, we have considered many aspects of the theory of neutrino mass and we have also studied some low-energy phenomena associated to massive neutrinos. These had to do with neutrino propagation *in vacuo* and in matter, as well nuclear beta and double-beta decays. So far, our discussion did not specify any particular gauge field theoretic origin for neutrino mass. In the next chapter, we will address the issue of analysing various alternative types of neutrino mass generation mechanisms. In particular, we will study the celebrated seesaw mechanism, the most popular mechanism by which neutrinos acquire masses. For definiteness and generality, we will first consider theories based on the simplest $SU(3)_c \otimes SU(2)_L \otimes U(1)_Y$ gauge group.

6.10 Problems for Chapter 6

6.1 Verify Eq. (6.34) using the symmetric parametrization of the lepton mixing matrix as well as the PDG presentation.

6.2 Show that the $0\nu\beta\beta$ decay rate is expected to be large if the mass spectrum is almost degenerate, even in the presence of the Majorana CP phases.

6.3 Consider the Feynman diagram analogous to that in the lower-right panel in Figure 6.8 but within the simplest $SU(3)_c \otimes SU(2)_L \otimes U(1)_Y$ model, where all fermion states are left-handed and the triplet is the one introduced in Eq. (7.1) in Chapter 7. Show that this 'left-handed' graph leads to a tiny $0\nu\beta\beta$ contribution, highly suppressed by the smallness of neutrino masses. Hint: analyse carefully the Higgs scalar sector formed by the isotriplet and standard isodoublet scalars.

6.4 Consider the scheme with neutrino masses induced by the two-loop level graph in Figure 6.11a. Show that, up to a logarithmic factor, one has, schematically,

$$\mathcal{M}_\nu \sim \lambda_0 \left(\frac{1}{16\pi^2}\right)^2 f Y_l h Y_l f^T \frac{\langle \Phi \rangle^2}{(m_k)^2} \langle \sigma \rangle, \tag{6.39}$$

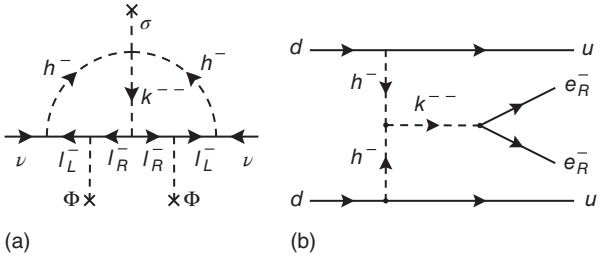

Figure 6.11 (a) Two-loop origin for neutrino mass. (b) Scalar exchange diagram for $0\nu\beta\beta$ decay.

in the limit where the doubly charged scalar k is much heavier than the singly charged one. Here, l denotes a charged lepton, f and h are their Yukawa coupling matrices and Y_l denotes the Higgs Yukawa couplings to charged leptons and $\langle\sigma\rangle$ is the singlet vacuum expectation value (vev). Neutrino masses can be naturally small because of the two-loop factor and the presence of a product of five small Yukawa couplings. Show that, thanks to the anti-symmetry of the f Yukawa coupling matrix, one of the three neutrinos is massless.

6.5 Estimate the tree-level $0\nu\beta\beta$ decay amplitude due to the singly and Doubly charged scalar boson exchange, as indicated in Figure 6.11b and compare it with the standard light neutrino exchange mass mechanism contribution.